acta physica slovaca vol. 54 No. 3, 263 – 271 **June 2004**

DECAY OF H_3^+ DOMINATED LOW-TEMPERATURE PLASMA

P. Macko[†1], G. Bánó[‡2], P. Hlavenka[*], R. Plašil[*], V. Poterya[*], A. Pysanenko[*], K. Dryahina[*], O. Votava[#], J. Glosík[*3]

[*] *Charles University Prague, Mathematics and Physics Faculty, Department of Electronics and Vacuum Physics, V Holešovikách 2, Prague 8, Czech Republic*

[†] *Comenius University, Faculty of Mathematics, Physics and Informatics, Department of Plasma Physics, Mlynska dolina F2, 84248 Bratislava, Slovakia*

[‡] *Res. Inst. for Solid State Physics and Optics, HAS, Konkoly-Thege út 29-33, 1121 Budapest, Hungary*

[#] *J. Heyrovský Institute of Physical Chemistry, Academy of Sciences of the Czech Republic, Dolejškova 3, 182 23 Prague 8, Czech Republic*

Received 9 April 2003, accepted 20 April 2004

Decay studies were carried out in the afterglow of low temperature plasma generated by pulsed microwave discharge in He with small admixture of Ar and H_2. In such a mixture all ions formed during a microwave discharge are by ion-molecule reactions converted to H_3^+ ions. The decay of the H_3^+ dominated afterglow plasma was monitored by means of infrared cavity ring-down spectrometer (CRDS) employing a cw-diode laser. Measurements were carried out at temperature of $\sim$ 350 K and total pressure of 0.66–2.66 kPa. The CRDS signal on the ν_2= 3 $\leftarrow$ 0 transition of H_3^+ (observed at around 1.4 μm) was detected at different moments during the discharge afterglow. Knowing the absorption cross-section the evolution of the absolute number density of $H_3^+(\nu$=0) during the afterglow was determined. The recombination rate coefficient calculated from the decay curves (at hydrogen number density of $[H_2] = 3–8\times10^{20}$ m^{-3}) is $\alpha = (1.8\pm0.8)\times10^{-13}$ m^3 s^{-1}. The absorption spectra provided us the kinetic temperature of $H_3^+(\nu$=0) ions during discharge and the afterglow. Detailed description of the experimental set up is also given here.

PACS: 52.38.Dx, 42.62.Fi

1 Introduction

The recombination of $H_3^+(\nu$=0) ions with electrons is an important ionisation loss process in natural and laboratory plasmas. $H_3^+(\nu$=0) ions were detected in interstellar clouds and in atmospheres of Jupiter, Saturn, Uranus and Neptune (see e.g. review by A. Dalgarno [1], and

[1] E-mail address: macko@fmph.uniba.sk
[2] E-mail address: bano@sunserv.kfki.hu
[3] E-mail address: Juraj.Glosik@mff.cuni.cz

review by T. Oka [2]). Despite the fact that the recombination of H_3^+ ions with electrons is one of the most studied recombination processes both experimentally and theoretically, the agreement between theory, experiment and astronomical observations was not achieved yet (see data and discussion in ref. [3-12]). Recombination rate-coefficient values reported in the literature differ by an order of magnitude. Our earlier stationary afterglow measurements [3,13,14] indicated that the recombination rate of H_3^+ depends on the partial pressure of H_2. At H_2 densities higher than 5×10^{18} m^{-3} the obtained effective recombination rate coefficient saturated at $\sim 1.2\times10^{-13}$ m^3 s^{-1}, while it dropped below 1×10^{-14} m^3 s^{-1} towards lower hydrogen densities ($< 10^{17}$ m^{-3}). The rate of H_3^+ recombination may depend strongly on the rotational and vibrational excitation level of the recombining ions. Our previous studies were carried out without identification of internal excitation of recombining ions (Langmuir probe was used for measurements of electron density).

Density of ions in a given vibrational and rotational level can be detected by spectroscopic absorption methods. Used method has to be very sensitive in order to monitor fast decay of ion density over several orders of magnitude with accuracy high enough to determine recombination rate coefficient. Infrared absorption was used by Amano [10] to obtain decay of $H_3^+(\nu{=}0)$ ions in the afterglow of pure hydrogen plasma at 27 – 80 Pa. Frequency-tuneable infrared laser and discharge cell with multitraversal mirrors were applied in the experiment. The recombination rate coefficient was determined to be $\alpha = (1.8\pm0.2)\times10^{-13}$ m^3 s^{-1} at 273 K. In this experiment also the temperature dependence of the recombination rate coefficient was observed in the range of 100–300 K. Fehér and co-workers also reported results of absorption measurements [15]. In this case, due to the low purity of the vacuum system, the obtained rate coefficient of 2×10^{-13} m^3 s^{-1} should be considered as an upper limit for the recombination of $H_3^+(\nu{=}0)$ with electrons at near thermal energies.

The aim of the present work is to start reinvestigation of the H_3^+ recombination with electrons in a well-defined internal state. For that reason we have built an infrared cw diode-laser cavity ring-down spectrometer (CRDS), that can measure the absolute value of number density of $H_3^+(\nu{=}0)$ in a plasma, both during the discharge and during the afterglow.

2 Principle of CRDS

Cavity Ring-Down Spectroscopy has been introduced in 1988 by O'Keefe and Deacon [16] as the technique allowing high-sensitivity absorption measurements using pulsed laser sources [17-19]. Even if pulsed lasers have the great advantage of a large spectral coverage (NIR to UV), they still remain expensive laboratory instruments. More recently, cw-CRDS technique was introduced functioning with cw single-frequency lasers [20-25]. The high sensitivity of the method is due to the enhancement of the effective optical path-length when laser light is reflected back and forth between the mirrors of the optical cavity. Prior to the detection of the ring-down signal the laser beam is coupled into the cavity through one of the mirrors. Using low-power cw diode lasers the intensity in the resonator becomes high enough only when the wavelength of the laser is matched to a given resonator mode. For that reason one of the cavity mirrors is usually placed on a piezoelectric transducer. This way periodical wavelength matching can be achieved by sweeping the length of resonator through the resonance position. Once the light intensity becomes high enough the laser beam is switched off and the decay of the light intensity (leaking through one of the

mirrors) is detected. Assuming linear absorption the decay is exponential with decay time $\tau(\nu)$, given by:

$$\frac{1}{\tau(\nu)} = \frac{1}{\tau_0} + \frac{d}{L}\, c\, \alpha(\nu). \tag{1}$$

ν is the frequency of the laser light, τ_0 is the decay time in the absence of absorption, d and $\alpha(\nu)$ are the length and absorption coefficient of the absorbing medium, respectively. L is the length of the cavity.

In the present experiments we used the experimental scheme of cw-CRDS developed by Romanini et al. [20,21]. We extended the method by the possibility of time-varying density measurement of absorbing species. The wavelength of the laser is tuned to the absorption lines of the overtone band $\nu_2 = 3 \leftarrow 0$ observed at around 1.4 μm [26]. Supposing the H_3^+ density to be of 10^{16} m^{-3} and temperature of 300 K the absorption coefficient of the strongest line of this band (at 6807.3 cm^{-1}) is about 10^{-5} m^{-1} (see line intensities given in [27,28]). This value is two orders of magnitude higher than the detection limit of CRDS, 10^{-7} m^{-1}, commonly achieved by mirrors having reflection of 99.995 %.

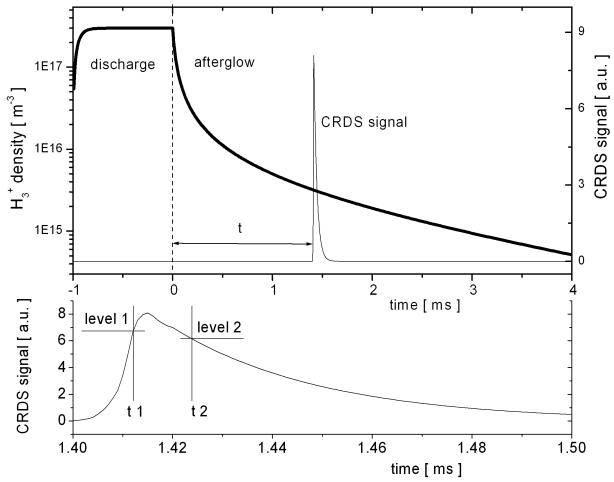

Fig. 1. Upper panel: Schematic data showing time dependence of the H_3^+ density during the discharge and the afterglow period. Simulated CRDS signal obtained with time delay of t (as compared to the moment when the discharge is switched off) is also shown. Lower panel: detailed view of the CRDS signal. The laser is switched off at the moment t_1, when the signal reaches level 1. Data acquisition starts at t_2, when the signal drops below level 2.

3 Experimental details

There are two possible operation regimes of the apparatus that can be used during the measurements. In first case the discharge operates continuously and the CRDS signal is detected at different laser frequencies. This way the absorption spectrum of the discharge is obtained. We use this regime to find the position of the H_3^+ absorption lines [26]. In the second case the discharge operates in pulsed regime and the time dependence of the H_3^+ density is obtained during the afterglow. For that the CRDS signal (belonging to a given absorption line) has to be detected with variable time delay t as compared to the moment when the discharge is switched off. The procedure is schematically shown in the upper panel of Fig. 1 and will be discussed later. As far as the temperature of the ions is constant during the afterglow period, it is enough to perform the measurements for the centre of the Doppler profile of the absorption line.

Figure 2 shows the schematic diagram of the experimental set-up. The microwave cavity is placed at the central part of the discharge tube (made of Pyrex with inner diameter of 40 mm). Plasma is generated by $\sim$ 1 ms long, microwave pulses (2.45 GHz) at repetition frequency of $\sim$ 220 Hz. Well-defined high voltage pulses are used to drive the magnetron. The effective length of the plasma column is estimated to be 50 mm. The microwave fall-off time in the cavity (after switching the magnetron off) is monitored by a high frequency diode D_3 that is placed in front of the cavity. During the afterglow the measured microwave signal decreases significantly within < 100 μs. In addition light emission from the discharge is monitored by an optical spectrometer that is equipped with a photo-multiplier tube. As an example we mention the spontaneous emission on a line around 900 nm (not identified) that decreases by two orders of magnitude within < 40 μs in the afterglow. In Fig. 3 microwave signal and signal corresponding to the light emission are plotted.

In Fig. 4 the kinetic temperature of the $H_3^+(\nu{=}0)$ during discharge and during very early afterglow is plotted. The kinetic temperature was determined from the Doppler broadening of the spectral line. During the microwave pulse kinetic temperature is ~ 350 K and it immediately decreases down to buffer gas temperature when microwaves are switched off. Actual wall temperature was ~ 320 K because of heating of the discharge tube by microwaves. At decay time > 50 μs the signal to noise ratio is so small that it is impossible to determine kinetic temperature, but there is no reason to assume that it will be different from the buffer gas temperature. The rotational temperature was also estimated by the comparison of line intensities corresponding to different rotational states. These measurements have low accuracy so we can only confirm that rotational temperature was close to 320 K, as one will expect in afterglow plasma at buffer gas pressure near to 1.33 kPa.

Used high purity gases pass through liquid nitrogen traps prior to entering the discharge tube. In the present experiments large flow of (99.999 grade) He is used to dilute eventual impurities desorbing from the walls. Mirrors of the optical cavity are placed at the end sides of the tube. To avoid deterioration of the mirrors by eventual plasma enhanced deposition, the discharge volume is separated from the mirror mounts by diaphragms of 6 mm diameter. Further suppression of the deposition is achieved by flow of gas (He) that enters the discharge tube nearby the mirrors and flows through diaphragms towards the discharge region by action of a large roots pump. Pressure of the gas in the discharge tube is measured by capacitance manometer. The composition of the gas mixture is controlled by MKS mass-flow-controllers. Typical conditions are as follows: He flow 0.67 Pa·m^{3}s^{-1} (400 sccm), Ar flow 5×10^{-3} Pa·m^3 s^{-1} (3 sccm), H_2

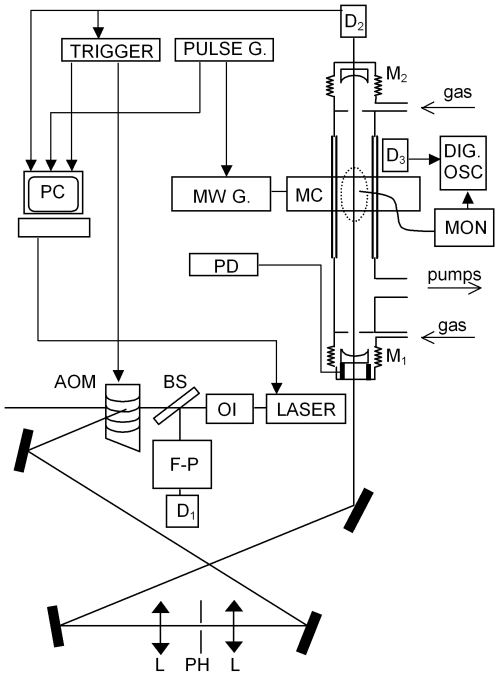

Fig. 2. The experimental set-up: OI – optical isolator, BS – beam-splitter, F-P Fabry-Perot interferometer, AOM – acousto-optical modulator, D_1 – InGaAs photodiode, D_2 – avalanche InGaAs photodiode, L – lenses, PH – pinhole, $M_{1,2}$ – dielectric mirrors, D_3 – high-frequency diode, MON – monochromator equipped with photomultiplier tube, PULSE G. – pulse generator, MW G. – microwave generator, PD – piezo-element driver, MC – microwave cavity.

flow $(0.83–1.67)\times10^{-3}$ Pa·m^3 s^{-1} (0.5–1 sccm).

The experimental set-up of cw-CRDS is also shown in Fig. 2. An external cavity single mode tuneable diode laser (Sacher Lasertechnik) with output power of about 3 mW is applied. The laser wavelength is tuneable by the external cavity in Littman configuration (from 1450 to 1480 nm). An optical isolator avoids re-injection of the reflected beam into the laser diode. Splitting up the beam, small part of the light is led into a Fabry-Perot interferometer (free spectral range of 3.33 GHz) that monitors the frequency shift during the measurements. The principal laser beam passes through an acousto-optic modulator (AOM) that is used to stop the propagation of the light towards the discharge tube. A space filter composed of two lenses and a pinhole of 50 μm is applied next. The first lens (focal length of 100 mm) focuses the laser beam onto the pinhole. A diaphragm that is placed after the pinhole selects the 0^{th} mode from the diffraction image. The second lens (focal length of 50 mm) matches the beam, having the free-space paraxial Gaussian-like profile, to the TEM_{00} mode of the cavity. The cavity is 710 mm long and is composed by two supermirrors having reflectivity of 99.995% around 1470 nm (Layertek, radius of curvature

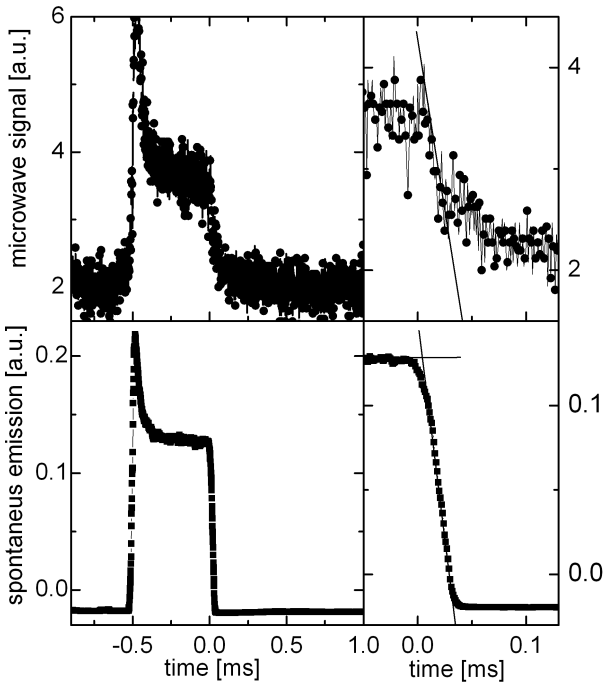

Fig. 3. Upper panel: Microwave signal obtained by fast diode placed close to the microwave cavity. The zero of the time scale is given to the time when voltage on the magnetron was switched off. The sharp peak at ~ 0.5 ms corresponds to high voltage peak deliberately given to the magnetron to ignite discharge. From the detail on the right side it is obvious that microwaves drops significantly within < 100 μs. Lower panel: Light emission detected in the 900 nm region. Again emission falls to zero within < 40 μs.

of 100 cm). One of the mirrors is mounted on a piezoelectric transducer in order to modulate the cavity length. This way the laser frequency can be periodically matched to one of the resonator's TEM_{00} modes.

The ringdown signal, transmitted through one of the cavity mirrors, is detected by an avalanche InGaAs photodiode D_2 and is amplified by a transimpedance amplifier (500 kΩ, bandpass up to 1 MHz). The signal is digitised with a 14 bits 2 MHz PC card (ADLink 2010). To observe clean ringdown decays, the laser beam is interrupted by the AOM once the signal of TEM_{00} mode transmission goes above a given threshold (level 1 in Fig. 2). Data acquisition starts when the signal drops below level 2 as indicated in Fig. 2. The laser frequency can be driven by a signal from the D/A converter of the ADLink 2010 PC card. The same card acquires the signal from the Fabry-Perot interferometer.

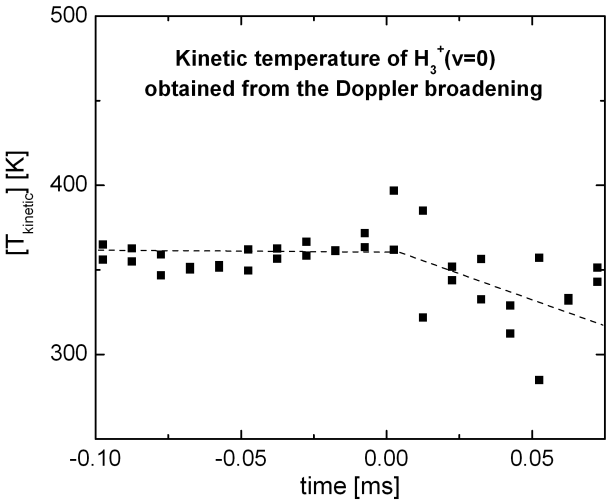

Fig. 4. Kinetic temperature of $H_3^+(\nu{=}0)$ as obtained from Doppler broadening of the spectral line.

4 Results

He^+, Ar^+, H^+ and H_2^+ ions are created in the discharge by electron impact. These ions are with nearly collisional rate ($\sim 10^{-15}$ m^3 s^{-1}) converted to H_3^+ by ion-molecule reactions with H_2 (sometime in several steps). If we assume that H_3^+ is recombining with rate coefficient $\sim 10^{-13}$ m^3 s^{-1}, we can find from balance equations that H_3^+ will be dominant ion in a steady state conditions of the discharge (shortly before switching microwaves off). When the microwaves are switched off fast electrons relax rapidly and production of energetic particles and ions is terminated. At hydrogen number densities $[H_2] \sim 10^{21}$ m^{-3} remaining ions are converted to H_3^+ within few microseconds. Since H_3^+ is the dominant ion already during the discharge period the absolute change of the H_3^+ density in the transition period from microwave discharge to afterglow is not very significant. Eventual formation of metastable particles during the discharge will not change substantially time scale of formation of H_3^+ because of fast penning ionisation at $[H_2] \sim 10^{21}$ m^{-3}. Taking into account the rate of the decrease of the microwave and light emission signal (Fig. 3), and the rate of formation of H_3^+ we can conclude that within < 50 μs H_3^+ ions are dominant in the afterglow. If we further consider that vibrationaly excited H_3^+(v) ions are deactivated in collisions with H_2 with rate coefficient $\sim 5{\times}10^{-17}$ m^3 s^{-1} than we can conclude that approximately 50 μs after discharge is switched off the afterglow plasma is dominated by $H_3^+(\nu{=}0)$ ions. This simple picture agrees with accurate calculation of the kinetics of formation of H_3^+ in the afterglow (see e.g. [3]).

Figure 5 shows a typical decay curve of the H_3^+ density. Assuming that during the afterglow period H_3^+ ions are lost from the volume by recombination and by diffusion to the walls, the time

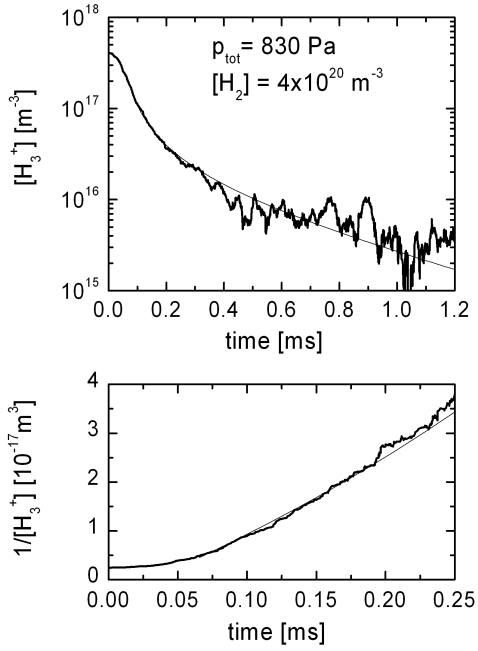

Fig. 5. Upper panel: Time dependence of the $H_3^+(\nu{=}0)$ density during the discharge afterglow. The fitted curve has the general shape given by equation (2). Lower panel: Detailed view of $1/[H_3^+(\nu{=}0)]$ in the early afterglow.

dependence of the ion density (in quasineutral conditions) can be expressed as:

$$[\mathrm{H}_3^+] = \left[\left(\alpha\cdot\tau_\mathrm{D} + \frac{1}{[\mathrm{H}_3^+]_0}\right) e^{\frac{t}{\tau_\mathrm{D}}} - \alpha\cdot\tau_\mathrm{D}\right]^{-1}, \tag{2}$$

where α is the recombination rate, τ_D is the characteristic diffusion time and $[\mathrm{H}_3^+]_0$ represents the density at $t = 0$. The corresponding fitted curve is also depicted in Fig. 5. The nearly linear time dependence of the reciprocal value of the H_3^+ density (see the detailed view in the lower panel of Fig. 5) indicates that recombination is the dominant loss process in the 0.08 – 0.2 ms time period. As an average result of many different data sets the recombination rate-coefficient was derived to be $(1.8\pm0.8)\times10^{-13}\mathrm{m}^3\ \mathrm{s}^{-1}$. This value belongs to hydrogen density of about $4\times10^{20}\mathrm{m}^{-3}$ and is in good agreement with our earlier values obtained in stationary afterglow measurements using a Langmuir probe [3,13,14].

Finally it is noted, that the characteristic ring-down time τ_0 in the empty resonator is $\sim 43\ \mu$s. It follows that the abrupt drop of the $H_3^+(\nu{=}0)$ density right after the discharge switches off cannot be reproduced by our simple evaluation method. A better iterative method was also tested, in which the changes of the H_3^+ density during the ring-down period were taken into account [29]. The results indicate that the corrections have only minor effect on the α values.

Acknowledgement: Thanks for financial support are due to GACR (205/02/0610, 202/02/0948), and MSM 1132000002. The experiments were carried out with support from EC's RTN under contract HPRN-CT-2000-0142, ETR and with support from Euroatom.

References

[1] Dalgarno: *Terrestrial and extraterrestrial H_3^+ in Advances in atomic, molecular, and optical physics* **32** (1994) 57

[2] T. Oka: *Am. Chem. S* **222** (2001) U208

[3] R. Plašil, J. Glosík, V. Poterya, P. Kudrna, J. Rusz, M. Tichý, A. Pysanenko: *Int. J. Mass Spectr.* **218** (2002) 105

[4] M.J. Jehnsen, H.B. Pederson, C.P. Safvan, K. Seiersen, X. Urbain, L.H. Andersen: *Phys. Rev. A* **6305** (2001) 2701

[5] D. Smith, P. Španěl: *Int. J. of Mass Spectr. and Ion Processes* **129** (1993) 163

[6] T. Gougousi, R. Johnsen, M.F. Golde: *Int. J. Mass Spectr. Ion Processes* **149/150** (1995) 131

[7] A. Canosa, B.R. Rowe, J.B.A. Mitchell, J.C. Gomet, C. Rebrion: *Astron. Astrophys.* **248** (1991) L19

[8] S. Laubé, A. Le Padellec, O. Sidko, C. Rebrion-Rowe, J.B.A. Mitchell, B.R. Rowe: *J. Phys. B: At. Mol. Opt. Phys.* **31** (1998) 2111

[9] V. Kokoouline, Chris H. Greene, B.D. Esry: *Nature* **412** (2001) 891

[10] T. Amano: *J. Chem. Phys.* **92** (1990) 6492

[11] T. Mosbach: *Inauguraldissertation*, Universitat Essen, 2002

[12] M. Larsson: *Phys. Trans. R. Soc. London A* **358** (2000) 2433

[13] J. Glosík, R. Plašil, V. Poterya, P. Kudrna, M. Tichý: *Chem. Phys. Letters* **331** (2000) 209

[14] J. Glosík, R. Plašil, V. Poterya, P. Kudrna, M. Tichý, A. Pysanenko: *J. Phys. B: At. Mol. Opt. Phys.* **34** (2001) L485

[15] M. Fehér, A. Rohrbacher, J.P. Maier: *Chem. Phys.* **185** (1994) 357

[16] A. O'Keefe, D.A.G. Deacon: *Rev. Sci. Instrum.* **59** (1988) 2544

[17] D. Romanini, L. Biennier, F. Salama, A. Kachanov, L.J. Allamandola, F. Stoeckel: *Chem. Phys. Lett.* **303** (1999) 165

[18] P. Macko, G. Counge, N. Sadeghi: *Europhysics Conference Abstracts, XVth ESCAMPIG Conference*, Lillafüred, Hungary, August 26 – 30, 2000

[19] P. Macko, G. Counge, N. Sadeghi: *J. Phys. D: Appl. Phys.* **34** (2001) 1807-1811

[20] D. Romanini, A.A. Kachanov, N. Sadeghi, F. Stoeckel: *Chem. Phys. Lett.* **264** (1997) 316

[21] D. Romanini, A.A. Kachanov, F. Stoeckel: *Chem. Phys. Lett.* **270** (1997) 538

[22] R. Engeln, G. von Helden, G. Berden, G. Meijer: *Chem. Phys. Lett.* **105** (1996) 262

[23] B.A. Paldus, C.C. Harb, T.G. Spence, B. Wilke, J. Xie, J.S. Haris, R.N. Zare: *J. Appl. Phys.* **83** (1998) 3991

[24] M. Murtz, B. Frech, W. Urban: *Appl. Phys. B* **68** (1999) 243

[25] Y. He, M. Hyppler, M. Quack: *Chem. Phys. Lett.* **289** (1998) 527

[26] P. Macko, R. Plašil, P. Kudrna, P. Hlavenka, V. Poterya, A. Pysanenko, G. Bánó, J. Glosík: *Czechoslovak Journal of Physics* **52** (Suppl. D 2002) D695

[27] L. Neale, S. Miller, J. Tennyson: *Astrophys. Journal* **464** (1996) 516

[28] T. Oka: *web page - http://h3plus.uchicago.edu/*

[29] P. Macko, G. Bánó, P. Hlavenka, R. Plašil, V. Poterya, A. Pysanenko, O. Votava, R. Johnsen, J. Glosík: *Int. J. Mass Spectr.* **233** (2004) 299